# Numerical Simulation of Hydrogen Bubble Growth at an Electrode Surface

Hongbo Liu, Liang-ming Pan* and Jian Wen

*Key Laboratory of Low-grade Energy Utilization Technologies and Systems (Chongqing University), Ministry of Education, Chongqing, 400044, China*

A single hydrogen bubble generated at an electrode surface during water electrolysis is simulated via the volume of fluid (VOF) multiphase flow model to capture the details of the interface evolution and the mass transfer that occurs at the interface. The hydrogen bubble that grows at the electrode is driven by supersaturation of the dissolved hydrogen in the liquid. Two models are used to calculate the gas-liquid interface mass transfer coefficient. The bubble growth from experimental results agrees closely with theoretical predictions. In addition, the mass transfer of dissolved hydrogen from the electrode surface to the bulk liquid is evaluated during the bubble nucleation and growth stages. During the nucleation stage, the mass transfer coefficient is $< 5.1 \times 10^{-5}$ m/s. Once the bubble embryo is formed, the mass transfer greatly increases. Before the bubble releases, the mass transfer coefficient reaches $2.8 \times 10^{-4}$ m/s. More detailed information about the bubble growth is presented, including bubble-induced convection and the concentration distribution of dissolved hydrogen around the growing bubble. The results indicate that the VOF method is suitable and reliable for simulating bubble behaviour during electrolysis or other electrochemical reactions that involve gas bubble desorption.

**Keywords:** hydrogen bubble evolution, CFD, VOF, interfacial mass transfer, water electrolysis

## INTRODUCTION

Bubble management is an important issue for all processes wherever they occur. During water electrolysis for hydrogen production, bubble evolution at the electrode surface has multiple effects on the electrochemical process. On one hand, the gas bubbles sticking to the nucleation sites block the electrode, decreasing the active surface and electrolyte conductivity.[1–4] On the other hand, momentum exchange and mass transfer occur between the bubbles and the surrounding electrolyte as the bubbles grow and are released.[5,6]

The bubble embryo forms on the electrode once the radius of the nucleus becomes greater than the critical point,[7,8] and it is then driven by the supersaturation of the dissolved gas to form a larger bubble.[9] Before the bubble reaches its release diameter, it might not detach into the electrolyte.[7] Before a new bubble forms at the nucleation site, it usually undergoes a nucleation stage. The duration of the nucleation time is different with various experiment conditions. For example, a relatively long time is required for a new bubble to form on smooth electrode surfaces.[9,10] However, the nucleation time is nearly zero for bubble nucleation at hydrophobic sites.[11]

Bubble evolution brings about microconvection,[12] and changes the concentration field within the supersaturation layer; in turn, the altered fields affect bubble behaviour.

Experimental research has focused on the behaviour of the bubble population near the macro-electrode,[13,14] and single bubble evolution at the micro-electrode surface.[15,16] This experimental method is reliable, and macroscopic variables, such as bubble diameter, velocity, and bubble-induced electrode potential fluctuation, are easily obtained. In contrast, it is difficult to obtain more locally detailed information about bubble growth processes, such as bubble-scale convection and the distribution of the concentration of dissolved substances around the growing bubble, to facilitate a thorough understanding of the process of gas bubble evolution. The currently existing simulation approach and calculation model, which emphasize the macro parameters based on assumptions about the mixture, cannot provide local information about bubble behaviour or the concentration distribution.[17–19]

In the last decade, numerical simulations have been extensively employed to investigate two-phase flow during flow boiling. A series of methods, such as volume of fluid (VOF),[20–22] level-set,[23–25] Lattice-Boltzmann (LB),[26–28] and phase-field,[29] were adopted to numerically investigate bubble growth, bubble detachment, and coalescence. In particular, VOF coupled with the Piecewise Linear Interface Calculation (PLIC) interface tracking method and the Continuum Surface Force (CSF) method was established as the method of choice.[22] Due to its numerical stability and computational efficiency, it was adopted for the simulation of boiling flows.[30] Kunkelmann and Stephan[31] studied the implementation and validation of a nucleate boiling model in the volume-of-fluid solver of OpenFOAM. The author has done many studies concerning bubble behaviour in subcooling flow boiling.[32–34] The analogy of the boiling process with gas evolution in electrochemical reactors is an attractive procedure to transfer insights obtained in one field to the other.[35] Kang[36] simulated gas-liquid interface evolution in the channels of direct methanol fuel cells (DMFC) with the VOF method. Xu[37] presented computational fluid dynamic (CFD) simulations to portray the flow characteristics in an air-lift bioreactor. However, the corresponding simulations of gas bubble desorption were sparse, especially for bubble growth relating to inter-phase mass transfer.

* *Author to whom correspondence may be addressed.*
*E-mail addresses: cneng@cqu.edu.cn*
Can. J. Chem. Eng. 94:192–199, 2016

DOI 10.1002/cjce.22378
Published online 25 November 2015 in Wiley Online Library (wileyonlinelibrary.com).

In this paper, a new approach that emphasizes interfacial transportation is implemented via the VOF method in a two-dimensional axisymmetrical domain to simulate single hydrogen bubble growth at the electrode surface. The local gas-liquid mass transfer rate is calculated based on the supersaturation model. Detailed information about bubble evolution is presented. The mass transfer coefficient related to the transport of dissolved hydrogen from the electrode surface to the bulk liquid is calculated.

## ELECTROCHEMICAL SIMPLIFICATION AND THE VOF MODEL

The purpose of this study is to compute a numerical solution for the growth of a bubble adhering to the electrode surface in water electrolysis. Bubble growth is driven by the supersaturation of dissolved gas around the bubble. The bubble consumes the dissolved hydrogen in the liquid that is produced by electrochemical reactions at the electrode surface following Faraday's law,[38] $J = \frac{MI}{2(1-\vartheta)F}$. This process is equivalent to a source of dissolved hydrogen existing at the active surface of the electrode. For simplicity, assumptions are made about both hydrodynamic and electrical problem solution procedures to place the principal focus on the aspects of concern.

1. Only the transportation of dissolved hydrogen species produced at the electrode surface by the electrochemical reaction is considered.
2. The production rate of dissolved hydrogen at the electrode surface of non-bubble coverage is uniform, following Faraday's law.
3. Heat exchange is neglected, and therefore the energy equation is not considered; it is assumed that the temperature is uniform.

For the transportation of dissolved hydrogen in the solution, the species transport equation is necessary.

$$\frac{\partial}{\partial t}(\rho Y_i) + \nabla \cdot \rho(\boldsymbol{u} Y_i - D_i \nabla Y_i) = S_i \tag{1}$$

where $Y_i$ is the mass fraction of species $i$, $D_i$ is the diffusion coefficient of species $i$, and $S_i$ is the source term due to heterogeneous reactions at the electrode surface. Under galvanostatic electrolysis, the source term, $S_i$, can be calculated following Faraday's law.

The VOF method was used to calculate the two-phase flow and to track the interface evolution, using the CFD software Fluent.[36] The volume fraction is used to distinguish each phase in the computational cell volume in the VOF method and can be expressed as follows:

$$\alpha_q = \begin{cases} 1 \ (\text{filled with q}^{\text{th}} \text{ phase}) \\ 0 \ (\text{not filled with q}^{\text{th}} \text{ phase}) \\ 0 \sim 1 \ (\text{interface}) \end{cases} \tag{2}$$

In this simulation, only the gas and liquid phases exist. For each computational cell, if it is not occupied by the gas phase, it must be occupied by the liquid phase. The sum of gas and liquid volume fractions is unity. An additional continuity equation for the volume fraction is necessary to calculate the volume fraction of each phase in the control volumes.

$$\frac{\partial \rho_q \alpha_q}{\partial t} + \nabla \cdot (\mathbf{u}_q \rho_q \alpha_q) = S_q \tag{3}$$

where $S_q$ is the mass source due to mass transfer between the liquid and gas phases.

The two phases share the same momentum equation:

$$\frac{\partial(\rho \mathbf{u})}{\partial t} + \nabla \cdot (\rho \mathbf{u}\mathbf{u}) = -\nabla p + \nabla \cdot \left[\mu(\nabla \mathbf{u} + (\nabla \mathbf{u})^{\mathrm{T}}) - \frac{2}{3}\mu \nabla \cdot \mathbf{u}\mathbf{I}\right] + \rho \mathbf{g} + \mathbf{F}_{\boldsymbol{\sigma}} \tag{4}$$

where the density is calculated by the weighted average $\rho = \alpha_g \rho_g + \alpha_l \rho_l$. $\mathbf{F}_\sigma$ is the surface tension expressed as a form of the volumetric effect; it is also a source term, N/m$^3$. In this paper, the surface tension was represented using a continuum surface force (CSF) model, and the expression obtained when only two phases are present in a cell is:

$$F_\sigma = \sigma \frac{\rho \kappa_q \nabla \alpha_q}{0.5(\rho_l + \rho_g)} \tag{5}$$

where σ is the interfacial tension between the liquid and gas and $\rho$ is the volume-averaged density of the cell. The curvature κ is defined in terms of the divergence of the unit normal $\hat{\mathrm{n}}$:

$$\kappa = \nabla \cdot \hat{\mathrm{n}} = \nabla \cdot \frac{\mathrm{n}}{|\mathrm{n}|} \tag{6}$$

The surface normal $\mathbf{n}$ is defined as the gradient of $\alpha_\mathrm{q}$, where $\alpha_\mathrm{q}$ is the volume fraction of the $q^{\text{th}}$ phase.

$$\mathrm{n} = \nabla \cdot \alpha_q \tag{7}$$

The curvatures of the $q^{\text{th}}$ phase, $\kappa_q$, are defined as:

$$\kappa_q = \nabla \cdot \hat{\mathrm{n}} = \nabla \cdot \frac{\mathrm{n}}{|\mathrm{n}|} = \nabla \cdot \frac{\nabla \alpha_q}{|\nabla \alpha_q|} = \frac{\Delta \alpha_q}{|\Delta \alpha_q|} \tag{8}$$

Due to the adhesion of fluids to the wall, the normal surface for cells near the wall is determined by considering the dynamic contact angle $\theta$:[39]

$$\hat{\mathrm{n}} = \hat{\mathrm{n}}_\mathrm{w} \cos\theta + \hat{\mathrm{t}}_\mathrm{w} \sin\theta \tag{9}$$

where $\hat{\mathrm{n}}_\mathrm{w}$ and $\hat{\mathrm{t}}_\mathrm{w}$ are the unit vectors normal and tangential tensor to the wall, respectively.

The Geometric Reconstruction Scheme (GRS) is used to track the dynamics of the gas bubble interface in Fluent. A user-defined function (UDF) was programmed to calculate the dissolved hydrogen production rate on the electrode surface based on Faraday's law. The parameters used here are the same as those in Glas and Westwater,[10] as shown in Table 1.

## INTERPHASE MASS TRANSFER

Multiple mass transfers happen simultaneously close to the electrode surface in water electrolysis,[40] including mass transport from the electrode surface to the bulk liquid and the permeation of dissolved substances through the gas bubble wall. The mass transfer coefficient is determined in terms of the Sherwood number and is used to characterize the source term in the phase transport equation.

### Sherwood Number $\mathrm{Sh}_1$

The mass transfer coefficient of the dissolved gas between the electrode surface and the bulk liquid is determined in terms of the

**Table 1**. Parameters used in this simulation

| Parameters[10] | Value |
|---|---|
| Electrolysis solution | 0.5 mol/L $H_2SO_4$ |
| Diffusion coefficient of $H_2$ ($D$) | $7.38 \times 10^{-9}$ $m^2/s$ |
| Surface tension ($\sigma$) | 0.075 N/m |
| Solution density ($\rho_l$) | 1000 $kg/m^3$ |
| Hydrogen gas density ($\rho_g$) | 0.09 $kg/m^3$ |
| Saturation of $H_2$ | $1.5e \times 10^{-6}$ kg/kg |
| Current density ($I$) | 410 $A/m^2$ |
| Electrode diameter | 0.127 mm |
| Operation temperature ($T$) and pressure ($p$) | 28 °C, 101 kPa (1 atm) |
| Nucleation waiting time | 30 s |
| Contact angle[a] ($\theta$) | Interpolation based on experimental data |

[a] $\theta = 2.581\,997 \times 10^{-7} \cdot R_{eq}{}^4 - 5.218\,877 \times 10^{-5} \cdot R_{eq}{}^3 + 3.676\,108 \times 10^{-3} \cdot R_{eq}{}^2 - 0.113\,933 \cdot R_{eq} + 1.962\,84$, $R_{eq}$ is bubble equivalent radius ($10^{-6}$ m), $R_{eq} = R((2 + 3\cos\theta - \cos^3\theta)/4)^{1/3}$, R is the bubble radius recorded in experiment ($10^{-6}$ m)

Sherwood number $Sh_1$. During the nucleation stage, because no bubble exists at the electrode surface, mass transfer depends on the free convection induced by the density gradient of the solution adjacent to the electrode. The single-phase free convection in electrolyte solution is expressed as:[41]

$$Sh_{1,f} \equiv \frac{k_f L}{D} = 0.64(GrSc)^{0.25} \tag{10}$$

which is restricted to laminar flow, where $L$ is the electrode dimension; the Grashof number is:

$$Gr = Ga\frac{\rho_\infty - \rho_e}{\rho_\infty} \tag{11}$$

$\rho_\infty$ is the bulk liquid density, and $\rho_e$ is the liquid density adjacent to the electrode. The average density of the liquid close to the electrode surface is used to calculate the Grashof number in the simulation. The Galileo number is:

$$Ga = \frac{gL^3}{\nu_L^2} \tag{12}$$

and the Schmidt number is:

$$Sc = \frac{\nu_L}{D} \tag{13}$$

Two types of microconvection influence the mass transfer of the dissolved substance once the bubble begins to grow at the electrode surface. The first is bubble-induced convection,[6,12] which is expressed by:

$$Sh_{1,b} \equiv \frac{k_b d}{D} = 1.89 \times \frac{(Ref_G)^{0.5} Sc^{0.487}[\vartheta^{0.5}(1 - \vartheta^{0.5})]^{0.5}}{1 - 2/3f_G} \tag{14}$$

where the Reynolds number is:

$$Re = \frac{I\varepsilon R_o T d}{(n_o/\nu)Fp\nu_L} \tag{15}$$

and the surface coverage is given by:

$$\vartheta = \left(\frac{d\sin(\theta)}{L}\right)^2 \tag{16}$$

The gas evolution efficiency[6,40,42] is defined as:

$$f_G = \frac{N_G}{N_T} \tag{17}$$

where $N_G$ is calculated from the gas bubble volume and $N_T$ is calculated from the current density following Faraday's law.

The second type of microconvection that influences the mass transfer of the dissolved substance is the single-phase free convection due to the concentration gradient around the bubble-attached electrode.[6,12] The dimensionless mass flux of the dissolved gas is given by:

$$Sh_{1,s} \equiv \frac{k_s d}{D} = 0.72\left(\frac{1 - \vartheta}{1 - 2/3f_G}\right)^{0.8}\left(\frac{j\varepsilon\alpha_o g L^4}{2F\nu_L^3}Sc^2\right)^{0.2} \tag{18}$$

where the expansion coefficient is:

$$\alpha_o = \left(13 + \frac{71}{1 - 2/3f_G}\right) \times 10^{-6} \tag{19}$$

The combined effect on mass transfer of both microconvections may be taken into account by:

$$k_e = (k_b^2 + k_s^2)^{0.5} \tag{20}$$

The mass transfer coefficient will be calculated within the entire lifetime of the bubble, including nucleation, bubble growth, and departure.

### Sherwood Number $Sh_2$

The mass transfer coefficient of the dissolved gas through the bubble wall is determined in terms of the Sherwood number $Sh_2$. Bubble growth is driven by the supersaturation of the dissolved substance. This supersaturation is given by $c_i - c_s$, where $c_s$ is the saturation concentration of dissolved hydrogen,[43] and $c_i$ is the concentration around the gas bubble interface. The mass transfer rate through the bubble surface, which refers to the source term in Equation (3), is expressed as follows:

$$\dot{m} = Mk_g(c_i - c_s) = \rho k_g(Y_i - Y_s) \tag{21}$$

where $k_g$ is the mass transfer coefficient through the gas bubble wall. The two models below are used to calculate the coefficient.

Model A is based on an empirical relation that is used to evaluate mass transfer through a spherical surface,[44,45] which has been adopted to calculate the mass transfer rate of bubbles adhering to the electrode cracks.[46]

$$Sh_{2,a} \equiv \frac{2k_a R}{D} = \left\{2 + 0.6\left(\frac{2Rv\rho}{\mu}\right)^{1/2}\left(\frac{\mu}{\rho D}\right)^{1/3}\right\} \tag{22}$$

where $\vec{v}$ is the liquid velocity around the sphere surface, $m \cdot s^{-1}$. For bubble growth in stagnant liquid, the velocity around the bubble wall is simplified as the moving velocity of the gas bubble interface, $v = \frac{dR}{dt}$.

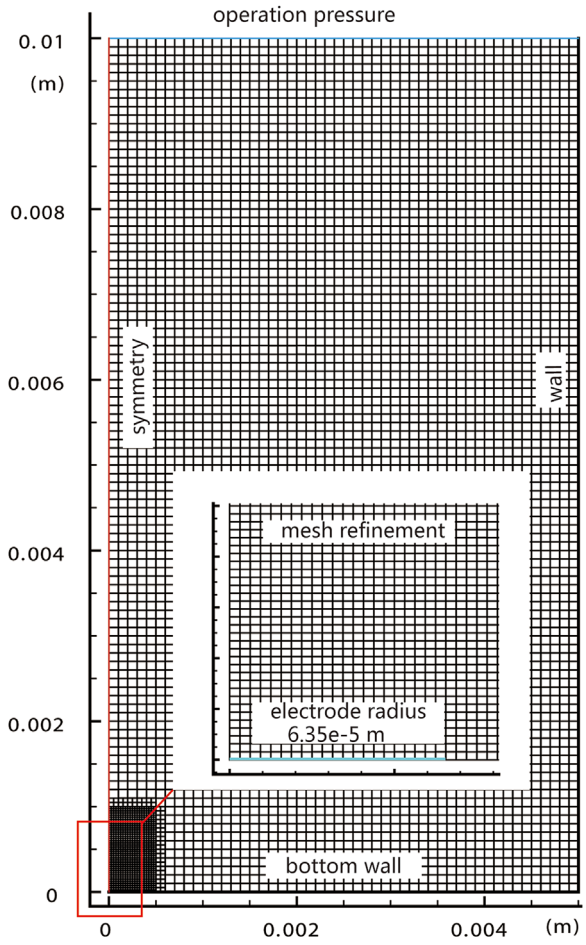


**Figure 1**. Calculation domain description and corresponding boundary conditions.

Model B, $Sh_{2,b} \equiv \frac{2k_bR}{D} = 2\left[1 + \frac{R}{(\pi Dt)^{0.5}}\right]$, comes from the analytical solution shown in Appendix A. In this simulation, $k_g$ is calculated following the two models above, and the results are shown in the next section.

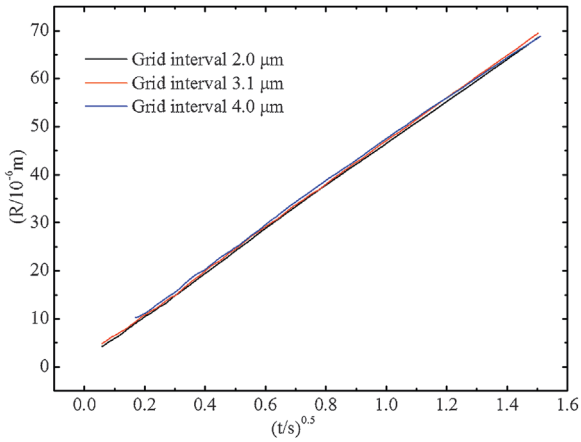


**Figure 2**. Grid intervals test for variation of bubble radius with square root of time.

## RESULTS AND DISCUSSION

A spherical bubble growing at the electrode surface can be simplified as an axisymmetrical problem, as depicted in Figure 1, assuming that a single bubble is nucleated at the electrode centre after the nucleation stage. The grids are tested with three intervals, 2, 3.1, and 4 μm, after refinement within the bubble growth domain (1 mm × 1 mm). The bubble growth lines under various grid intervals are shown in Figure 2.

Bubble evolution includes two different stages, nucleation and growth. The nucleation waiting time is necessary until the bubble embryo forms at the electrode surface, so the numerical simulation is performed in two steps. Initially, before the bubble is generated, the electrolytically-developed hydrogen dissolves into the liquid adjacent to the electrode. If the local concentration exceeds a threshold value, nucleation will occur at cavities of the electrode surface. The local supersaturation before nucleation at the electrode surface can be calculated as $c_i - c_s = \frac{2\sigma}{R'}\frac{c_s}{P}$, where $R'$ is the critical radius of curvature of the meniscus of the cavity.[9] Nucleation time is most strongly correlated with current density and electrode surface condition. At the same time, the same current density may result in variation of the nucleation waiting time if the experiment is conducted with different electrodes. A

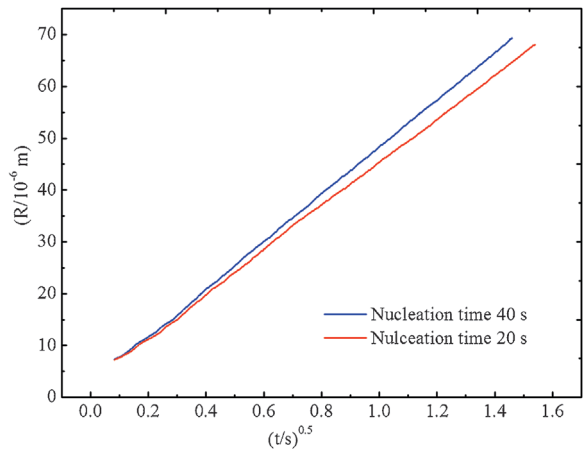


**Figure 3**. Bubble growth rate comparison under different nucleation times.

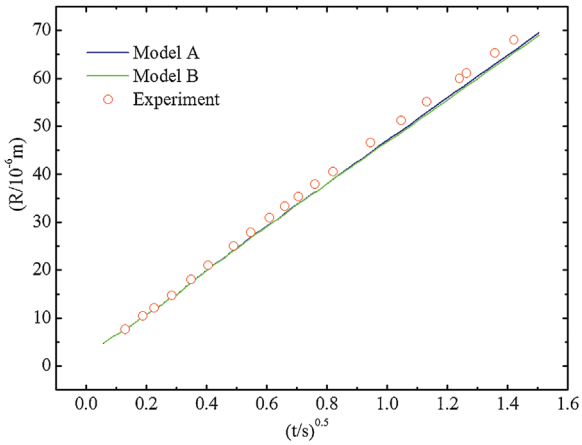


**Figure 4**. Variation of bubble radius with square root of time; comparison of different models with the experiment data.

longer nucleation waiting time leads to greater supersaturation of dissolved hydrogen in the electrolyte, which might result in faster growth of the bubble embryo. In this study, a comparison of bubble growth is made using two different nucleation times, 20 and 40 s, as shown in Figure 3. The results show that a longer nucleation time results in faster growth of the bubble embryo, which matches the theoretical prediction.

After the nucleation waiting time, i.e. the nucleation stage, a bubble embryo is formed at the electrode surface in the experiment. In this simulation, the gas volume fraction of several computational cells close to the electrode surface is set to one after the nucleation stage, simulating the initial embryo. The nucleation time here is the same as in the experimental results,[10] as shown in Table 1. Scriven[47] published a model of a bubble limited by the diffusion of the dissolved gas, $R = 2\beta(Dt)^{1/2}$, where $D$ is the diffusion coefficient of the dissolved molecular gas and $\beta$ is a current-dependent growth coefficient. In this simulation, the bubble volume is monitored over time. The bubble equivalent radius, $R_{eq} = \left(\frac{3V}{4\pi}\right)^{1/3}$, is calculated to adjust the dynamic contact angle following the equation shown in Table 1. The bubble radius is recorded as $R = \left(\frac{V}{f}\right)^{1/3}$, where $f = \frac{\pi}{3}(2 + 3\cos\theta - \cos^3\theta)$, and the results are shown in Figure 4. Both Models A and B are suitable for calculating the gas bubble interface mass transfer, and the simulation of bubble growth shows close agreement with experimental data and the theoretical model.

Bubble detachment from the surface occurs when the balance is broken between the forces that maintain it on the electrode and the forces that release it. These various forces include drag, surface tension, inertial pressure, and buoyancy forces.[9] In boiling heat transfer, the break-off diameter is usually calculated from the Fritz relationship,[48,49] $R_d = 0.0104\theta\sqrt{\frac{\sigma}{(\rho_l - \rho_g)g}}$, while reliable results for the release diameter prediction of an electrolysis bubble have not yet been obtained, for three possible reasons. The first reason is that the disturbance caused by neighbouring bubbles results in premature departure from the electrode surface.[50] The second reason is that the variation of wetting conditions is expressed by the contact angle, controlled by the liquid-electrode interfacial tension that depends on the potential. This effect is known as

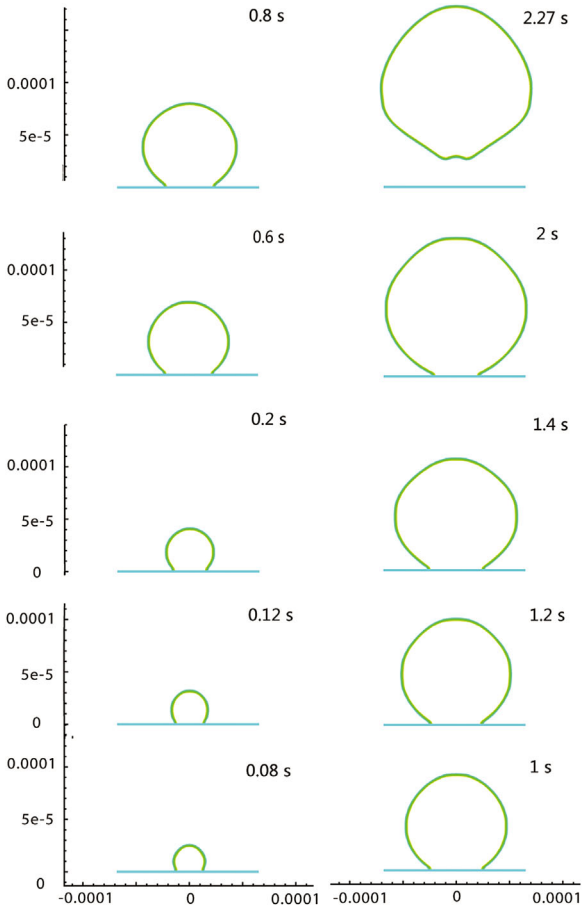


**Figure 5**. Gas bubble interface evolution with time. Blue straight line indicates electrode size 0.127 mm.

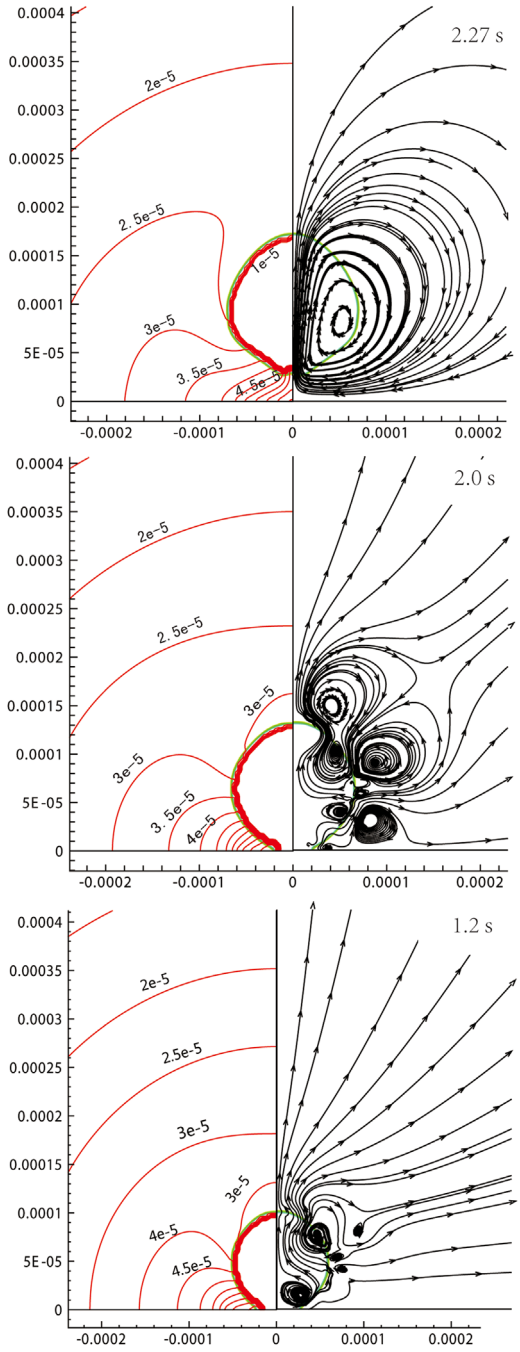


**Figure 6**. Concentration distribution (mass fraction, %) of dissolved hydrogen (left part) and the streamlines evolution (right part) around the growing bubble.

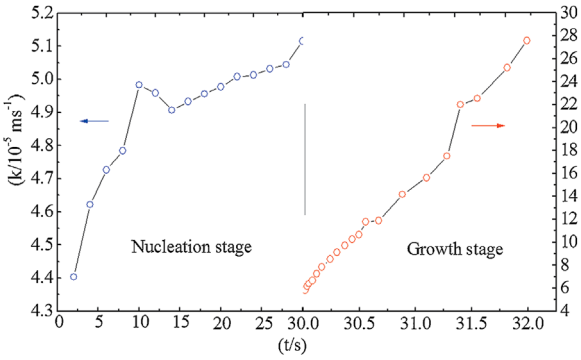


**Figure 7**. Variation of mass transfer coefficient for dissolved hydrogen gas within nucleation and growth stages respectively.

electrocapillarity. The last possible reason is the variation of surface tension in the presence of dissolved gas.[51,52] In this simulation, the bubble growth and release are shown in Figure 5, and the release radius is approximately 69 μm.

The emergence and evolution of gas bubbles at the electrode surface bring the influence on the mass transfer of the dissolved substance from the electrode surface to the bulk liquid. Before bubble nucleation, dissolved hydrogen is enriched around the electrode surface as electrolysis proceeds. The liquid density gradient brings about free convection. Once the bubble embryo begins to grow, its surface pushes out the surrounding liquid, which brings about bubble scale microconvection, as shown in Figure 6. The movement of the bubble surface causes non-uniform shear force for the fluid element around the interface, which induces evolution of the vortexes as the bubble grows. The vortexes in the liquid facilitate dissolved gas transport from the electrode surface to the bulk liquid.

The quantification of the influence of bubble evolution on mass transfer is shown in Figure 7. During the nucleation stage, the mass transfer coefficient grows rapidly at first, and then the increase begins to flatten, reaching $< 5.1 \times 10^{-5}\,\mathrm{m \cdot s^{-1}}$ by the end of the stage. The bubble evolution at the surface changes the relatively low mass transfer coefficient at the beginning. As the bubble grows, the coefficient becomes much larger, up to $2.8 \times 10^{-4}\,\mathrm{m \cdot s^{-1}}$, until the bubble is released.

## CONCLUSIONS

In this study, more local information about bubble growth, including bubble-induced convection and concentration distribution, was obtained via the VOF method. The results indicate that the models of gas-liquid interface mass transfer used in this paper are suitable and reasonable. During the nucleation stage, free convection induced by a concentration gradient plays an important role in the facilitation of mass transfer from the electrode surface to the bulk liquid. In the bubble growth stage, mass transfer is greatly increased and peaks before the bubble is released from the electrode surface. Bubble formation removes the dissolved hydrogen from the electrode surface, and the induced microconvection increases mass transfer from the surface to the bulk liquid. More detailed information is presented that describes bubble-induced convection and facilitates a deeper understanding of gas desorption in water electrolysis. This is a first attempt to demonstrate the suitability of the VOF method for studying bubble evolution problems in electrochemical processes. This model and method can be used for further relevant studies.

## ACKNOWLEDGEMENTS

The authors are grateful for the support of the Natural Science Foundation of China (Grant no. 51376201).

## NOMENCLATURE

| | |
|---|---|
| $A$ | area of gas bubble surface ($m^2$) |
| $c$ | concentration of dissolved hydrogen ($mol/m^3$) |
| $d$ | bubble release diameter (m) |
| $D$ | diffusion coefficient ($m^2/s$) |
| $F$ | Faraday constant |
| $g$ | acceleration due to gravity ($m/s^2$) |
| $I$ | current density ($A/m^2$) |
| $J$ | dissolved hydrogen production rate ($kg/(m^2 s)$) |
| $k$ | mass transfer coefficient (m/s) |
| $\dot{m}$ | mass transfer rate ($kg/(m^2 \cdot s)$) |
| $M$ | molar mass (kg/mol) |
| $n_o$ | charge number |
| $N_G$ | flux density of bubbles adhering to the electrode ($mol/(m^2 \cdot s)$) |
| $N_T$ | flux density of formation of dissolved gas at electrode surface ($mol/(m^2 \cdot s)$) |
| $p$ | operation pressure (Pa) |
| $R$ | bubble radius (m) |
| $R_d$ | bubble departure radius (m) |
| $R_o$ | universal gas constant (8.314 J/(mol·K)) |
| $t$ | time (s) |
| $T$ | temperature (K) |
| $\boldsymbol{u}$ | velocity (m/s) |
| $V$ | gas bubble volume ($m^3$) |
| $Y_i$ | species mass fraction |

### Greek Letters

| | |
|---|---|
| $\alpha_q$ | void fraction of $q$ phase |
| $\beta$ | growth coefficient |
| $\varepsilon$ | current efficiency |
| $\vartheta$ | bubble coverage fraction of electrode |
| $\nu$ | stoichiometric number |
| $\mu$ | viscosity ($kg/(m \cdot s)$) |
| $\nu_L$ | kinematic viscosity ($m^2/s$) |
| $\theta$ | bubble contact angle (rad) |
| $\sigma$ | interfacial tension (N/m) |
| $\rho$ | density ($kg/m^3$) |

### Subscripts

| | |
|---|---|
| $g$ | gas phase |
| $l$ | liquid phase |
| $q$ | $q^{th}$ phase, $g$ or $l$ |

## APPENDIX A

The model was derived by Cheh and Tobias[53] and is summarized here. For a growing bubble adhering to the electrode surface, the diffusion of dissolved hydrogen in spherical coordinates can be written as:

$$\frac{\partial c}{\partial t} = \frac{D}{r^2}\frac{\partial}{\partial r}\left(r^2 \frac{\partial c}{\partial r}\right) \tag{A.1}$$

with the bubble centre as the origin of a spherical coordinate system and $r$ as the distance from the origin.

Under the assumption of a uniform concentration distribution around the bubble, the boundary and initial conditions are given as:

$$\begin{aligned} &c(R,t) = c_s, t > 0 \\ &c(r,t) = c_i, t > 0, r \to \infty \\ &c(r,0) = c_i, r > R \end{aligned} \tag{A.2}$$

By introducing the variable $c^* = r(c - c_s)$, Equation (A.1) can be written as:

$$\frac{\partial c^*}{\partial t} = D\frac{\partial^2 c^*}{\partial r^2} \tag{A.3}$$

where the boundary conditions are:

$$\begin{aligned} &c^*(R,t) = 0, t > 0 \\ &c^*(r,0) = r(c_i - c_s), t > 0, r \to \infty \\ &c^*(r,0) = r(c_i - c_s), r > R \end{aligned} \tag{A.4}$$

Defining $r^* = r - R$, a solution can be given as:

$$c^*(r,t) = \frac{c_i - c_s}{2\sqrt{\pi D t}} \int_0^\infty (R + r^{*\prime}) \Big\{ \exp[-(r^* - r^{*\prime})^2/4Dt] - \exp[-(r^* + r^{*\prime})^2/4Dt] \Big\} dr^{*\prime} \tag{A.5}$$

Following Equation (A.5), the concentration gradient at the bubble surface, $r = R$, can be written as:

$$\left(\frac{\partial c^*}{\partial r}\right)_{r=R} = (c_i - c_s)\left\{1 + \frac{R}{\sqrt{\pi D t}}\right\} \tag{A.6}$$

and:

$$\left(\frac{\partial c}{\partial r}\right)_{r=R} = (c_i - c_s)\left\{\frac{1}{R} + \frac{1}{\sqrt{\pi D t}}\right\} \tag{A.7}$$

For a growing bubble, the mass balance that exists at the surface can be expressed as:

$$\rho_g \frac{dV}{dt} = AD\left(\frac{\partial c}{\partial r}\right)_{r=R} \tag{A.8}$$

Combining Equations (A.7, A.8), the averaged mass transfer flux through the bubble surface is:

$$\dot{m} = D\left(\frac{\partial c}{\partial r}\right)_{r=R} = \frac{D}{R}\left[1 + \frac{R}{(\pi D t)^{0.5}}\right](c_i - c_s) \tag{A.9}$$

Following Equation (A.9), the mass transfer coefficient of model B is given as:

$$Sh_{2,b} \equiv \frac{2k_b R}{D} = 2\left[1 + \frac{R}{(\pi D t)^{0.5}}\right] \tag{A.10}$$

## REFERENCES


[1] H. Vogt, *Electrochim. Acta* **1980**, *25*, 527.

[2] P. J. Sides, C. W. Tobias, *J. Electrochem. Soc.* **1980**, *127*, 288.

[3] P. Byrne, P. Bosander, O. Parhammar, E. Fontes, *J. Appl. Electrochem.* **2000**, *30*, 1361.

[4] J. Dukovic, C. W. Tobias, *J. Electrochem. Soc.* **1987**, *134*, 331.

[5] E. Delnoij, J. A. M. Kuipers, W. P. M. van Swaaij, *Chem. Eng. Sci.* **1999**, *54*, 2217.

[6] H. Matsushima, D. Kiuchi, Y. Fukunaka, K. Kuribayashi, *Electrochem. Commun.* **2009**, *11*, 1721.

[7] S. F. Jones, G. M. Evans, K. P. Galvin, *Adv. Colloid Interfac.* **1999**, *80*, 27.

[8] M. E. Tawfik, F. J. Diez, *Electrochim. Acta* **2014**, *146*, 792.

[9] S. F. Jones, G. M. Evans, K. P. Galvin, *Adv. Colloid Interfac.* **1999**, *80*, 51.

[10] J. P. Glas, J. W. Westwater, *Int. J. Heat Mass Tran.* **1964**, *7*, 1427.

[11] C. Brussieux, P. Viers, H. Roustan, M. Rakib, *Electrochim. Acta* **2011**, *56*, 7194.

[12] H. Vogt, *Electrochim. Acta* **1993**, *38*, 1421.

[13] T. Weier, S. Landgraf, *Eur. Phys. J.-Spec. Top.* **2013**, *220*, 313.

[14] H. Matsushima, T. Iida, Y. Fukunaka, *J. Solid State Chem.* **2012**, *16*, 1421.

[15] D. Fernández, M. Martine, A. Meagher, M. E. Möbius, J. M. D. Coey, *Electrochem. Commun.* **2012**, *18*, 28.

[16] G. Sakuma, Y. Fukunaka, H. Matsushima, *Int. J. Hydrogen Energ.* **2014**, *39*, 7638.

[17] P. Maciel, T. Nierhaus, S. V. Damme, H. V. Parys, J. Deconinck, A. Hubin, *Electrochem. Commun.* **2009**, *11*, 875.

[18] S. Karagadde, S. Sundarraj, P. Dutta, *Scripta Mater.* **2009**, *61*, 216.

[19] K. Aldas, *Appl. Math. Comput.* **2004**, *154*, 507.

[20] L. M. Pan, T. C. Jen, C. He, M. D. Xin, Q. H. Chen, *J. Heat Transf.* **2006**, *128*, 838.

[21] Z. Yang, X. F. Peng, P. Ye, *Int. J. Heat Mass Tran.* **2008**, *51*, 1003.

[22] R. Zhuan, W. Wang, *Int. J. Heat Mass Tran.* **2010**, *53*, 502.

[23] A. Mukherjee, S. G. Kandlikar, *Int. J. Heat Mass Tran.* **2007**, *50*, 127.

[24] G. Son, V. K. Dhir, *Int. J. Heat Mass Tran.* **2008**, *51*, 2566.

[25] S. van der Pijl, A. Segal, C. Vuik, P. Wesseling, *Comput. Visual. Sci.* **2008**, *11*, 221.

[26] A. Gupta, R. Kumar, *Int. J. Heat Mass Tran.* **2008**, *51*, 5192.

[27] N. Takada, M. Misawa, A. Tomiyama, S. Fujiwara, *Comput. Phys. Commun.* **2000**, *129*, 233.

[28] Z. L. Yang, T. N. Dinh, R. R. Nourgaliev, B. R. Sehgal, *Int. J. Therm. Sci.* **2000**, *39*, 1.

[29] Y. Sun, C. Beckermann, *Physica D* **2008**, *237*, 3089.

[30] J. H. Wei, L. M. Pan, D. Q. Chen, H. Zhang, J. J. Xu, Y. P. Huang, *Nucl. Eng. Des.* **2011**, *241*, 2898.

[31] C. Kunkelmann, P. Stephan, *Numer. Heat Tr. A-Appl.* **2009**, *10*, 631.

[32] D. W. Yuan, L. M. Pan, D. Q. Chen, H. Zhang, J. H. Wei, Y. P. Huang, *Appl. Therm. Eng.* **2011**, *31*, 3512.

[33] L. M. Pan, Z. W. Tan, D. Q. Chen, L. C. Xue, *Nucl. Eng. Des.* **2012**, *248*, 126.

[34] L. M. Pan, J. W. Deng, D. W. Yuan, D. Q. Chen, J. Q. Zhang, *Sci. China Ser. E-Technol. Sci*. **2009**, *52*, 2967.
[35] H. Vogt, *Int. J. Heat Mass Tran*. **2013**, *59*, 191.
[36] S. Kang, B. Zhou, *Int. J. Hydrogen Energ*. **2014**, *39*, 2325.
[37] Y. Y. Xu, L. J. Luo, J. Q. Yuan, *Can. J. Chem. Eng*. **2011**, *89*, 360.
[38] H. Vogt, J. Eigeldinger, *Electrochim. Acta* **2000**, *45*, 4449.
[39] J. U. Brackbill, D. B. Kothe, C. Zemach, *J. Comput. Phys*. **1992**, *100*, 335.
[40] H. Vogt, *Electrochim. Acta* **1984**, *29*, 167.
[41] A. A. Wragg, *Electrochim. Acta* **1968**, *13*, 2159.
[42] H. Vogt, *Electrochim. Acta* **1984**, *29*, 175.
[43] D. Kashchiev, A. Firoozabadi, *J. Chem. Phys*. **1993**, *98*, 689.
[44] R. B. Brid, W. E. Stewart, E. N. Lightfoot, *Transport Phenomena*, 2nd edition, Wiley, New York **1960**.
[45] E. L. Cussler, *Diffusion: Mass Transfer in Fluid Systems*, 3rd edition, Cambridge University Press, New York **2009**.
[46] Y. Tanaka, S. Uchinashi, *Electrochim. Acta* **2003**, *48*, 4013.
[47] L. E. Scriven, *Chem. Eng. Sci*. **1959**, *10*, 251.
[48] W. Fritz, *Phys. Z*. **1935**, *36*, 379.
[49] C. W. M. P. Sillen, E. Barendricht, L. J. J. Janssen, S. J. D. van Stralen, *Int. J. Hydrogen Energ*. **1982**, *7*, 577.
[50] R. J. Balzer, H. Vogt, *Electrochim. Acta* **2005**, *50*, 2073.
[51] Z. B. Li, B. C. Y. Lu, *Chem. Eng. Sci*. **2001**, *56*, 2879.
[52] S. D. Lubetkin, M. Akhtar, *J. Colloid Interf. Sci*. **1996**, *180*, 43.
[53] H. Y. Cheh, C. W. Tobias, *Int. J. Heat Mass Tran*. **1968**, *11*, 709.

*Manuscript received January 5, 2015; revised manuscript received April 8, 2015; accepted for publication April 27, 2015.*